IEEE Access
Multidisciplinary | Rapid Review | Open Access Journal

Received September 11, 2021, accepted October 20, 2021, date of publication October 26, 2021,
date of current version November 8, 2021.

Digital Object Identifier 10.1109/ACCESS.2021.3122954

Direct Power Based Control Strategy for DAB DC-DC Converter With Cooperative Triple Phase Shifted Modulation

YONG DAI[1], SUHUA LUO[2], AND ZHONGWEI LI[3], (Member, IEEE)
[1]School of Mechatronics Engineering, Harbin Institute of Technology, Harbin 150001, China
[2]School of Physics, Harbin Institute of Technology, Harbin 150001, China
[3]School of Electrical Engineering and Automation, Harbin Institute of Technology, Harbin 150001, China

Corresponding author: Zhongwei Li (lzw@hit.edu.cn)

ABSTRACT The cooperative triple-phase-shifted modulation (CTPS) for the isolated dual-active bridge (DAB) DC-DC converter has the advantages of zero dual-DC side flow back currents and best current characteristics. However, the mathematical model and corresponding closed-loop control configuration of the DAB converter driven by CTPS are not presented so far. In order to solve this problem, in this paper, the average state space model of the DAB converter driven by CTPS is established for the first time. It is proven that the DAB converter driven by CTPS is a zero-order system and it is not necessary to construct an inner inductor current closed-loop control loop in the entire closed-loop control configuration of DAB converter. Furthermore, the average power model is derived. Two control strategies based on the resulted average power model when the DAB converter is connected to DC microgrid or a pure resistive load are proposed to realize the precise control of the transfer power or the output voltage, respectively. The detailed experimental results verify the correctness of the established mathematical model and the closed-loop control strategies.

INDEX TERMS Closed-loop control, direct power control, dual active bridge DC-DC converter, triple phase shift.

I. INTRODUCTION

The isolated dual active bridge (DAB) DC-DC converter has the advantages of bidirectional power flow and bidirectional boost/buck voltage conversion, and fast dynamic response. Due to these advantages, the DAB DC-DC converter has been widely applied in the fields of the renewable energy generation systems and the energy storage systems, microgrids, solid state transformer, aerospace, fuel cells generation system, and so on [1]–[6].

Nowadays, towards increasing the comprehensive performance of DAB converter, the researchers focus on the full soft-switching realization, the optimization of current characteristics, including reducing the current stress and real mean square (RMS) value of the inductor current and the closed-loop control strategies. In [7]–[9], the current stress is discussed and corresponding improvement methods are proposed. In [10], the current characteristics is discussed and a current characteristics optimization is proposed to improve the efficiency and reduce the current stress. In [11], [12], the problem of flow back current, which is also defined as the circulating current or nonactive current, is discussed and several solutions are proposed.

The existing literatures mainly concern the improvement of some certain key problems of DAB converter mentioned above, however, these strategies cannot solve all of the above problems. In [13], a cooperative triple-phase-shifted modulation (CTPS) is proposed to realize the basic voltage/power conversion and at the same time, to eliminate the dual-DC sides flow back currents and minimize the current stress of the power switches and RMS value of the inductor current. Eliminating the dual-side flow back currents is helpful to reduce the DC side current ripples and minimizing the RMS value of the inductor current is helpful to increase the efficiency. Furthermore, under the same maximum transfer power, the current stress of the CTPS is not greater than the SPS and as a result, the CTPS is much better than the SPS in terms of the current characteristics, efficiency and cost.

More importantly, in the actual industrial applications, the DAB DC-DC converter is usually controlled with the closed-loop configuration to achieve a better dynamic response and precise steady-state control performance.

The associate editor coordinating the review of this manuscript and approving it for publication was Yuh-Shyan Hwang.

In order to analysis the open-loop characteristics and design the closed-loop controller parameters, the small-signal models of DAB DC-DC converters have been built and some linear control methods have been adopted based on the small-signal models. In [14], [15], a full-order model taking into account the leakage inductance current and the resonant transition intervals is built. In [16], a full-order continuous-time average model using the dc terms and first order terms of transformer current is built. In [17], the small-signal model of DAB converter based on the generalized state space average modeling method is built.

Some closed-loop control strategies are also proposed to improve the performance of the DAB DC-DC converter. In [18], [19], a model-based phase-shift control has been proposed to improve the dynamic characteristics in the load disturbance conditions. In [20], the model prediction control method is introduced into DAB converter to increase the dynamic performance. In [21], when the step change of the current reference occurs, the inductor current peak value corresponding to the new current reference is calculated based on the inductor current expressions and used to control the actual inductor current to obtain a good dynamic performance. In [22], the expression of average transfer power as a function of outer phase shift with the single-phase-shifted modulation (SPS) is derived to calculate the actual phase shift according to the power reference. In this way, the small-signal model is not used and in theory, the dynamic performance keeps constant in the entire power range because the actual performance is in independent of the pre-chosen operation point, which is necessary in the small-signal model based control system. In [23], [24], the interconnection and damping assignment passivity based control is applied to the port-controlled hamiltonian model of DAB converter in a DC Microgrid. In [25], an improved instantaneous current control for three-phase DAB converter is proposed.

Generally, the mathematical model of the DAB converter is related to the modulation strategies adopted. The previously presented models are all based on SPS. The resulted small-signal models are not able to directly apply in the DAB converter driven by CTPS because its characteristics are quite different from the SPS based ones. However, the linear model of the CTPS based DAB converter are not presented so far.

Similarly, all of the presented closed-loop control strategies are based on the SPS and they are not able to be applied in the DAB converter driven by CTPS.

In order to realize combining the CTPS with the closed-loop control system, it is necessary to build the mathematical model of the DAB converter driven by the CTPS and to propose some more closed-loop control strategies.

In this paper, the mathematical model and corresponding closed-loop control strategy of the DAB converter driven by the CTPS are researched originally. The innovation and contribution of this paper are as follows. (1) The average state-space model of the DAB converter with the CTPS is originally derived. It is proven that it is a zero-order system if neglecting the effect of secondary DC capacitor. (2) Based on the zero-order system characteristics, the control strategies of the DAB converter when it is connected to a DC microgrid or serves alone as a DC source supply are proposed based on the obtained power model, on the one hand, to realize the precise control of the transfer power and output voltage, on the second hand, to simplify the closed-loop control configuration and reduce the design burden of the controller parameters.

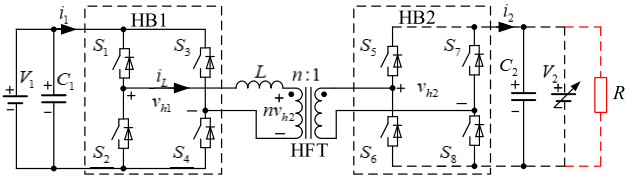

FIGURE 1. Schematic of isolated DAB DC-DC converter.

II. BRIEF INTRODUCTION TO CTPS

Fig. 1 shows the schematic of the DAB DC-DC converter, where HB1 and HB2 are the two H-bridge converters; v_{h1} and v_{h2} are the AC side output voltages of HB1 and HB2, respectively; i_1 and i_2 are the DC side currents of HB1 and HB2, respectively. n is the turns ratio of HFT and i_L is the DC inductor current. Fig. 2 shows the operating waveforms of the general TPS modulation in the scenario that the power flows from V_1 to V_2 and $V_1 \geq nV_2$. In Fig. 2, the inner phase shift ratios of HB1 and HB2 are defined as D_1 and D_2, respectively; and the outer phase shift ratio between v_{h1} and v_{h2} is defined as D_φ.

The flow back current is briefly discussed below. Assuming that the power transfers from V_1 to V_2, the ideal situation is that both the primary DC side current flowing through V_1 to HB1 and the secondary DC side current flowing through HB2 to V_2 should be not less than zero. Otherwise, if i_1 or i_2 is less than zero in some regions, the power will be transferred back from HB1 to V_1 or from V_2 to HB2 for a short time during the switching period. This part current is defined as the flow back current and it is not expected. The negative effect of the flow back currents have been described in detail in [13] and it is not mentioned here. CTPS in [13] is proposed to not only eliminate the dual-DC sides flow back currents, but also optimize the current characteristics and achieve the full soft switching in the entire power range.

The principle of the CTPS is briefly explained here. The details please refer to [13]. Fig. 2(a) shows the operating waveforms of the CTPS. i_1 and i_2 are never less than zero in the entire switching period and the flow back currents are eliminated. From [13], the relationship between the three phase shifts in order to eliminate the dual-side flow back currents can be expressed as

$$D_2 = D_\varphi = 1 + k\,(D_1 - 1) \tag{1}$$

where $k = V_1/nV_2$ is the voltage conversion ratio.

If it is assumed k is greater than 1, when D_2 is equal to 1, D_1 is less than 1 and the corresponding operating waveforms of the CTPS are shown in Fig. 2(b). This point is called the critical point. In [13], the corresponding D_1 and the average

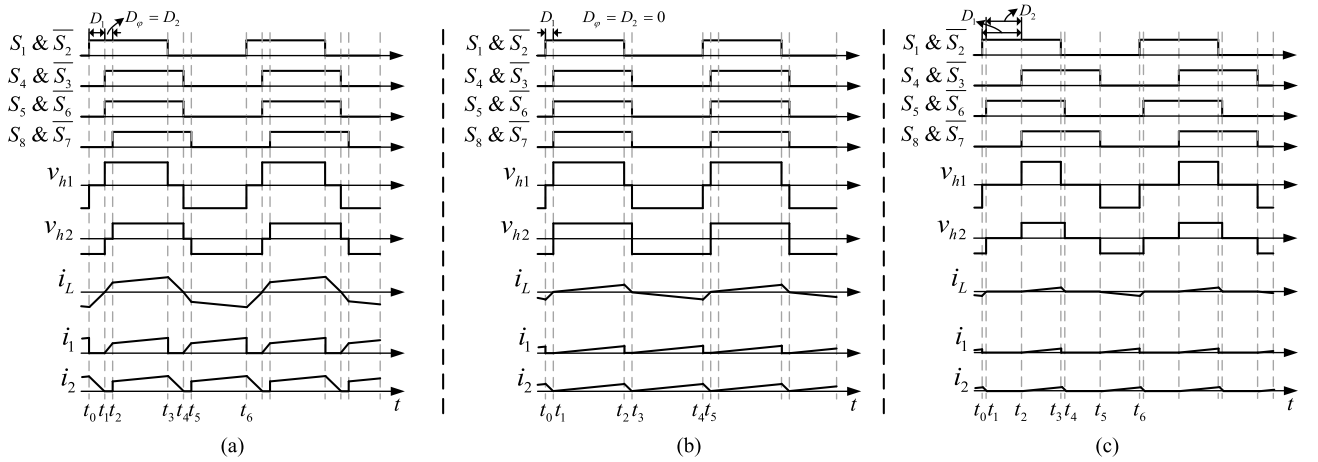

FIGURE 2. Operating waveforms of proposed CTPS. (a) $P_{av} > P_{av\_cri}$, (b) Critical point$P_{av} = P_{av_cri}$, and (c) $P_{av} < P_{av\_cri}$.

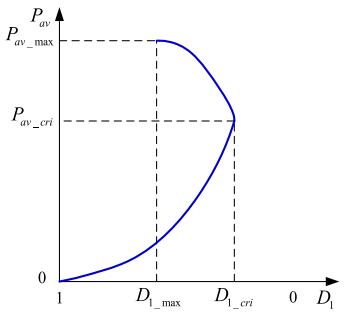

FIGURE 3. Distribution curve of average power as a function of D_1 in CTPS.

power at the critical point (P_{av_cri}) have been solved and are expressed as

$$D_{1\_cri} = \frac{(k-1)}{k} \tag{2}$$

$$\begin{cases} P_{av\_cri} = \dfrac{V_1^2 T_s}{4Lk^2}\left(1-\dfrac{1}{k}\right) \\ p_{av\_cri} = \dfrac{P_{av\_cri}}{\frac{V_1 n V_2 T_s}{8Lk^2}} = \dfrac{2}{k}\left(1-\dfrac{1}{k}\right) \end{cases} \tag{3}$$

where p_{av_cri} is the per-unit value of P_{av_cri}.

When $P_{av} < P_{av\_cri}$, D_φ should keep equal to zero and the relationship between D_1 and D_2 is the same as that in (1). The corresponding operating waveforms are shown in Fig. 2(c).

The relationship between D_φ and D_1 in the entire power range can be expressed as

$$D_\varphi = \begin{cases} D_2 = 1 + k\,(D_1 - 1)\,, & P_{av} \geq P_{av\_cri} \\ 0, & P_{av} < P_{av\_cri} \end{cases} \tag{4}$$

When the relationship between the three phase shifts meet (3), P_{av} can be expressed as (5) (shown at the bottom of the page).

From [13], the maximum average power and D_1 at the maximum average power point can be expressed as

$$P_{av\_\max} = \frac{V_1^2 T_s}{4L}\frac{1}{k^2+k+1} \tag{6}$$

$$D_{1\_\max} = \frac{k^2}{k^2+k+1} \tag{7}$$

It has been indicated in [13] that, when $P_{av} \geq P_{av\_cri}$, D_1 should be tuned in the region of $[D_{1\_cri}, D_{1\_\max}]$ to obtain a good current characteristics. Similarly, when $P_{av} < P_{av\_cri}$, D_1 should be tuned in the region of $[D_{1\_cri}, 1]$.

The distribution curve of the average power as a function of D_1 is drawn and shown in Fig. 3. When D_1 is tuned in the region of $[D_{1\_\max}, 1]$, the relationship between the average power and D_1 is not of one-to-one correspondence. In addition, the exact value of D_φ is also determined by the actual average power. Therefore, the desired average power instead of D_1 is chosen as the input of CTPS. The actual expression of D_1 as a function of P_{av} is derived from (4) and it is shown below.

When $p_{av} \geq p_{av\_cri}$, the actual expression of D_1 as a function of p_{av} is

$$D_1 = \frac{k^2}{k^2+k+1} - \sqrt{\frac{k}{k^2+k+1}\left(\frac{1}{k^2+k+1} - \frac{p_{av}}{2k}\right)} \tag{8}$$

When $p_{av} < p_{av\_cri}$, the expression of D_1 is

$$D_1 = 1 - \sqrt{\frac{p_{av}}{2k-2}} \tag{9}$$

$$P_{av}(D_1) = \begin{cases} \dfrac{V_1^2 T_s}{4L}\left[\dfrac{1}{k^2+k+1} - \dfrac{k^2+k+1}{k}\left(D_1 - \dfrac{k^2}{k^2+k+1}\right)^2\right], & P_{av} \geq P_{av\_cri} \\ \dfrac{V_1^2 T_s}{4L}\left(1-\dfrac{1}{k}\right)(1-D_1)^2\,, & P_{av} < P_{av\_cri} \end{cases} \tag{5}$$

III. AVERAGE STATE-SPACE MODEL OF DAB CONVERTER WITH CTPS

In this section, the average state-space model of DAB converter with CTPS is derived first. The reason why uses this kind of modelling method is explained below. It is because that during each positive-half switching period, the inductor current always starts at zero and ends at zero. It means the operation process in the positive-half switching period is decoupled from that in the negative-half switching period.

In addition, since the starting and ending values of all the variables, including the inductor currents and voltages across it are known, only the average model of the converter in the positive-half period needs to build. Thus the problem existed in the conventional SPS or DPS does not exist. As a result, the average state-space modelling method can be applied in the CTPS based DAB converter. The resulted model by using this modelling method is precise because there is no any approximation is taken during the modelling process, which is usually necessary in the popular fundamental analysis method.

A. $P_{av} \geq P_{av\_cri}$

From Fig. 2(a), during $[t_1, t_2]$, the state space equation is

$$\begin{cases} L\dfrac{di_{L\_av}}{dt} = V_1 \\ C_2\dfrac{dV_2}{dt} = -\dfrac{V_2}{R} \end{cases} \tag{10}$$

where R is load resistance. During $[t_2, t_3]$, the state space equation is

$$\begin{cases} L\dfrac{di_{L\_av}}{dt} = V_1 - nV_2 \\ C_2\dfrac{dV_2}{dt} = ni_{L\_av} - \dfrac{V_2}{R} \end{cases} \tag{11}$$

During $[t_3, t_4]$, the state space equation is

$$\begin{cases} L\dfrac{di_{L\_av}}{dt} = -nV_2 \\ C_2\dfrac{dV_2}{dt} = ni_{L\_av} - \dfrac{V_2}{R} \end{cases} \tag{12}$$

The average state-space equation can be derived from (10)-(12) and it is expressed as

$$\begin{cases} L\dfrac{di_{L\_av}}{dt} = D_\varphi V_1 + \left(1 - D_1 - D_\varphi\right)(V_1 - nV_2) - D_1 nV_2 \\ = (1 - D_1)(V_1 - knV_2) \\ C_2\dfrac{dV_2}{dt} = \left(1 - D_1 - D_\varphi + D_1\right) ni_{L\_av} - \dfrac{V_2}{R} \\ = (1 - D_2)\, ni_{L\_av} - \dfrac{V_2}{R} \\ = i_{2\_av} - \dfrac{V_2}{R} \end{cases} \tag{13}$$

where i_{2_av} is the average value of secondary DC side current, which is proportional to the actual load.

By substituting $k = V_1/nV_2$ into (13), it yields

$$\begin{aligned} L\frac{di_{L\_av}}{dt} &= (1 - D_1)(V_1 - knV_2) \\ &\equiv 0 \end{aligned} \tag{14}$$

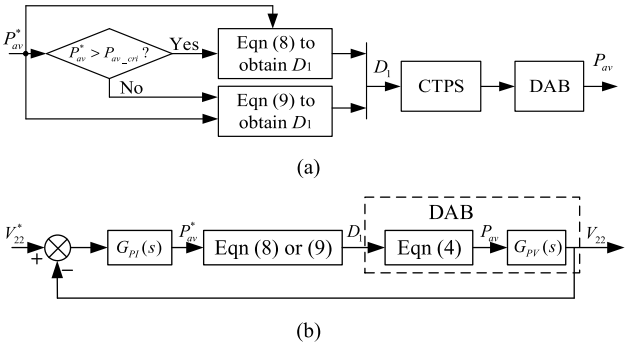

FIGURE 4. Control schematics of DAB DC-DC converter controlled by CTPS. (a) Single power loop, and (b) V_2 closed-loop control.

It means the transfer function of D_1 to i_L cannot be obtained from the average state space equation.

B. $P_{av} < P_{av\_cri}$

From Fig. 2(c), during $[t_2, t_3]$, the state space equation is

$$\begin{cases} L\dfrac{di_{L\_av}}{dt} = V_1 - nV_2 \\ C_2\dfrac{dV_2}{dt} = ni_{L\_av} - \dfrac{V_2}{R} \end{cases} \tag{15}$$

During the region of $[t_3, t_4]$, the state space equation is

$$\begin{cases} L\dfrac{di_{L\_av}}{dt} = -nV_2 \\ C_2\dfrac{dV_2}{dt} = ni_{L\_av} - \dfrac{V_2}{R} \end{cases} \tag{16}$$

The average state-space equation in a switching period is

$$\begin{cases} L\dfrac{di_{L\_av}}{dt} = (1 - D_1)(V_1 - nV_2) - (D_1 - D_2)\, nV_2 \\ = (1 - D_1)(V_1 - knV_2) \\ = 0 \\ C_2\dfrac{dV_2}{dt} = (1 - D_2)\, ni_{L\_av} - \dfrac{V_2}{R} \\ = (1 - D_2)\, ni_{L\_av} - \dfrac{V_2}{R} \\ = i_{2\_av} - \dfrac{V_2}{R} \end{cases} \tag{17}$$

From (13), (14) and (17), the unified average state-space model of the DAB converter with CTPS in the entire power range can be described in the following matrix form.

$$\frac{d}{dt}\begin{bmatrix} i_{L\_av} \\ V \end{bmatrix} = \begin{bmatrix} 0 & 0 \\ 0 & -\dfrac{1}{RC_2} \end{bmatrix}\begin{bmatrix} i_{L\_av} \\ V_2 \end{bmatrix} + \begin{bmatrix} 0 & 0 \\ 0 & 1 \end{bmatrix}\begin{bmatrix} V_2 \\ i_{2\_av} \end{bmatrix} \tag{18}$$

From the built average state-space model of DAB converter with CTPS, the derivative of the average inductor current in a switching period is always equal to zero. It is also independent of the input and output voltages and the variation of three phase shifts.

It means there is a certain relationship between the three phase shifts and the exact average inductor current in a switching period. As a result, the inductor current is directly determined by the phase shifts. In other words, when it is

desired to realize the step change of the transfer power, it can be realized by updating the corresponding phase shifts directly and the inductor current becomes the corresponding value immediately without any transient process. This unique feature leads to the following two merits of the DAB converter. The first one is that, there is no transient transition between the variation of phase shifts and the actual inductor current. The transient transition process mentioned here is the transient process of the actual inductor current from the initial steady state to the new steady state caused by the step change of the phase shifts or the input/output voltages. The second one is that the inductor current is always under control because it is always determined by the present phase shifts and input/output voltages. Therefore, even the inductor current is not specially considered in the entire closed-loop control system, it can still realize a good dynamic performance and the over-current problem existed in the common power electronics devices does not occur.

From this unique characteristics, it does not need to set a inductor current control loop in the entire control configuration of the DAB converter and the inductor current does not varies uncontrollably. This characteristic simplifies the closed-loop control configuration of the DAB converter.

IV. CLOSED-LOOP CONTROL STRATEGIES OF DAB CONVERTER WITH CTPS

Since it is not necessary to set an inductor current control loop in the DAB converter with CTPS. The closed-loop control of the DAB converter can be implemented in a simply way. From the actual application fields of the DAB converter, the DAB converter is possible to connect to the DC microgrid or works alone as a DC source supply. For the scenario of using in DC microgrid, V_2 is regarded as constant and only the transfer power should be controlled. If the DAB converter is used as a DC source supply, both the transfer power and the terminal DC voltage should be controlled. The control strategies of the two application scenarios are discussed separately.

A. DAB CONVERTER CONNECTED TO DC MICROGRID

In this scenario, V_2 is regarded as constant. Considered that the DAB DC-DC converter is usually used to connect the PV or battery to the DC microgrid. The single output/input power control approach is adopted. Known from the average state-space model, the DAB converter controlled by CTPS is a zero-order system and there is no transient process between the average transfer power or the inductor current and the phase shifts. It means that, when a certain phase shifts are applied to the DC-DC converter, the corresponding power can be achieved immediately. In this scenario, a simple power control approach is used and the schematic is shown in Fig. 4. The desired power is compared with the critical power first, if the desired power is larger than the critical power, the actual phase shift D_1 is determined by (8), otherwise, D_1 is determined by (9). Then D_2 and D_φ are calculated by (4). It should be indicated that, this system is essentially an open-loop system because the expressions of (8) or (9) used to calculate D_1 do not consider the power loss of the DAB converter. This method is still effective because even though there is the transfer power error, the controlled variables of the DC microgrid are still able to be controlled at their desired values because of the closed-loop control algorithm performed in the main control unit of DC microgrid.

B. DAB CONVERTER CONNECTED TO RESISTIVE LOAD

In this scenario, V_2 should be constant and the closed-loop control of V_2 is adopted. In addition, considering that when the power varies in the entire range, the variation of D_1 is not monotonous. D_1 cannot be determined directly by the controller output of V_2. The direct power control is still used in this scenario. The control loop of V_2 is set as the outer loop and the output of the V_2 control loop is set as the transfer power reference. Then the actual D_1 can be calculated from (8) or (9) and D_2 and D_φ are calculated from (4).

The transfer function of the transfer power to V_2 is derived as follows. The average transfer power in a switching period can be derived as

$$P_{av} = i_{2\_av} V_2 \tag{19}$$

$$i_{2\_av} = P_{av}/V_2 \tag{20}$$

Substituting (19) into (17), the differential equation of V_2 can be derived as

$$C_2 \frac{dV_2}{dt} = \frac{P_{av}}{V_2} - \frac{V_2}{R} \tag{21}$$

It can be further derived as

$$\frac{1}{2} C_2 \frac{dV_2^2}{dt} + \frac{V_2^2}{R} = P_{av} \tag{22}$$

Setting a new variable $V_{22} = V_2^2$ and the s-domain transfer function of the average power to V_{22} can be derived as

$$G_{PV}(s) = \frac{V_{22}}{P_{av}} = \frac{1}{\frac{C_2}{2}s + \frac{1}{R}} \tag{23}$$

Then the DAB DC-DC converter controlled by CTPS is equivalent to a first-order inertial element. In order to simplify the system, the controller of V_2 is set as a proportional-integral (PI) controller. The entire control approach in this scenario is drawn in Fig. 4(b).

The design of the PI controller parameters is descripted as follows. The closed-loop transfer function is

$$\begin{aligned} G_{PV\_close}(s) &= \frac{V_{22}}{V_{22}^*} = \frac{G_{PI}(s)G_{PV}(s)}{1 + G_{PI}(s)G_{PV}(s)} \\ &= \frac{K_p s + K_I}{s} \frac{1}{\frac{C_2}{2}s + \frac{1}{R} + \frac{K_p s + K_I}{s}} \end{aligned} \tag{24}$$

By using the principle of zero-pole points cancellation, the design rule of the coefficients of the PI controller is obtained. The proportional coefficient of V_2 controller is designed as $C_2/2$ and the integral coefficient is designed as $1/R_{rated}$, where R_{rated} is the rated load of the DAB converter. Then the final closed-loop transfer function yields

$$G_{PV\_close}(s) = \frac{1}{s+1} \tag{25}$$

TABLE 1. Values of experimental platform parameters.

Parameter	Value	Parameter	Value
V_1	100V	Range of p_{av}	0.2-0.55
V_2 (initial)	25V	Initial voltage ratio k	2
n	2:1	Load resistance	2.5Ω (rated)
Range of V_2	18V-25V	Output capacitance C2	470uF
T_s (f_s)	50us (20kHz)	K_p	235
L	100uH	K_I	1/2.5

It is obvious that the resulted transfer function is the first-order inertial element and it is unconditionally stable.

Since C_2 and R_{rated} are predesigned and are easy to obtain, the two coefficients are also easy to calculate.

V. EXPERIMENTAL RESULTS AND DISCUSSION

The experimental prototype of DAB DC-DC converter based on DSP chip TMS320F28335 is built as shown in Fig. 5 to validate the proposed control strategies. The experimental parameters are listed in Table 1. A DC source supply is connected to HB1 as the main power supply. A resistor and another DC source supply are connected to the DC side of HB2. The second DC source supply is used to emulate the DC microgrid. If it is assumed that the DAB converter serves as a DC source supply, the second DC source supply should be removed to ensure that only the DAB converter supplies the power to the load to evaluate its dynamic performance.

Considering that in the actual system, the phase shifts should vary in real time to tune the transfer power, the implementation of CTPS using the DSP chip is briefly described below. Fig. 6 illustrates the operating waveforms of the CTPS implemented by the DSP considering the update process of the phase shifts. The four timers T1-T4 in the DSP chip are synchronous and the phase shifts are updated by updating the various compare registers. At the starting moment of various timers, these registers are calculated and updated based on the new phase shifts.

In addition, the rising edges of the control signals of S_4 and S_8 always align at the starting moment of the timers. It ensures that the phase shifts are always updated at the zero-crossing point of the inductor current. From Fig. 6, If it is assumed that the phase shifts should be updated at t_k, the compare registers CR1A, B and CR4A, B are directly updated by replacing D_1 and D_φ by D_1' and D_φ' and anything else does not need to do. From Fig. 6, the actual phase shifts are equal to the desired ones immediately after the update moment without any delay or error. More importantly, there is no DC bias current caused during the transient process.

The experimental verification is performed in the following steps. First, the built average state-space model is verified via suddenly varying the unified average power reference from 0.2 to 0.55. In this case, the two DC side voltages

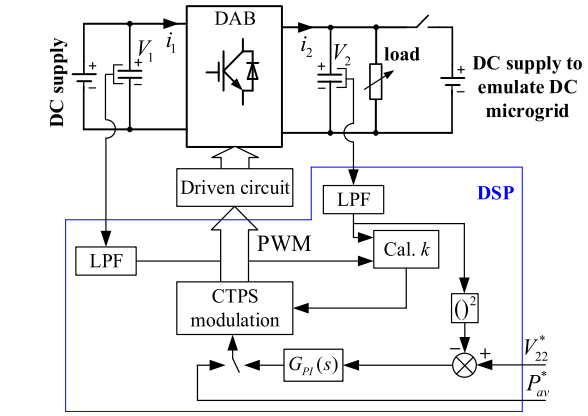

(a)

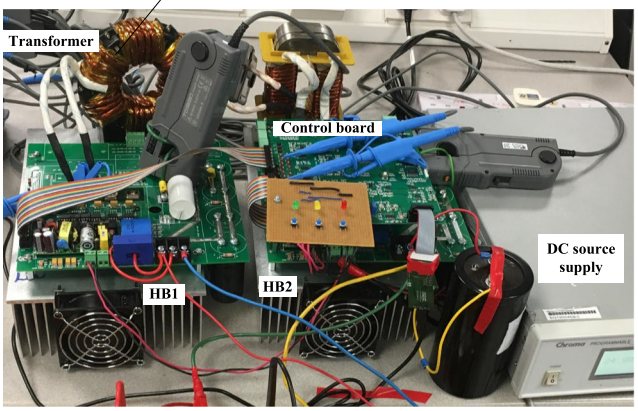

(b)

FIGURE 5. Schematic and photograph of experimental platform of DAB converter. (a) Schematic, and (b) Photograph.

V_1 and V_2 keep constant. The corresponding experimental waveforms are shown in Fig. 7. From Fig. 7(a), after the unified average power reference jumps from 0.2 to 0.55, the three phase shifts are calculated immediately based on the new power reference. The inductor current increases immediately and reaches its new steady state in the same switching period. There is no transient transition process in the inductor current. It can be easily verified by the profile of the inductor waveforms. Similarly, after the unified average power reference jumps from 0.55 to 0.2, as shown in Fig. 7(b), the inductor current decreases immediately and reaches to the new steady state without the transient process. It means the actual inductor current, but not its average derivate is directly determined by the phase shifts. For any phase shifts, there is a certain inductor current corresponding to them. These experimental results shown in Fig. 7 verify that the unique characteristics of DAB converter controlled by the CTPS, namely it is essentially a zero-order system. It means the built model is correct.

This unique feature significantly simplifies the closed-loop control configuration of the DAB converter. Furthermore, the corresponding waveforms of the averaged i_2 are also shown in Fig. 7. Due to the constant V_2, the averaged i_2 is proportional to the actual average transfer power. From Fig. 7(a) and (b), the averaged i_2 reaches its new steady state

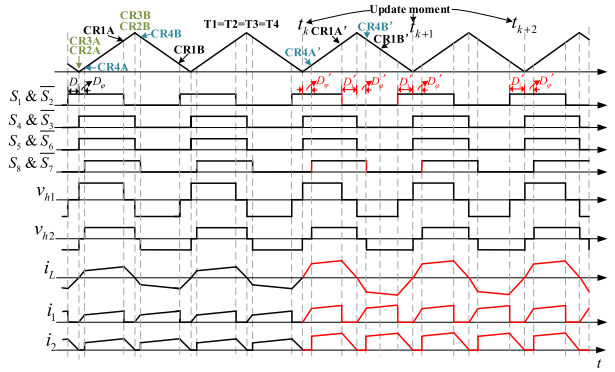

FIGURE 6. Transient waveforms of CTPS implemented by DSP.

value very fast after the step change of the power reference occur. The ratios between the initial and the final values of the averaged i_2 in these two scenarios are the same as those of the power reference. It means the desired transfer power are achieved. It should be indicated that the transfer power error is not seriously evaluated in this paper. The reason is power error can be compensated by higher-level closed-loop controller, i.e., the DC bus voltage closed-loop controller operated in the central control system of the DC microgrid.

Secondly, the dynamic performance of the DAB converter with secondary voltage closed-loop control approach is evaluated. In this situation, the second DC source supply is removed and only the resistor is connected to the DC side of HB2. Considering that the voltage closed-loop control approach should achieve the zero-steady state even under the conditions of the sudden changes of the voltage reference or the load resistance, it is verified in two separate ways.

The first way is that the voltage reference jumps from 18V to 25V and jumps back after a certain period. The corresponding experimental waveforms are shown in Fig. 8. In order to further verify the built average state model, the waveforms of the inductor current along with the controlled variable, namely V_2 and the averaged i_2 (denoting the transfer power) are all shown. From Fig. 8, in these two cases, after the voltage reference jumps, the actual inductor current and the averaged i_2 vary immediately and the actual secondary DC side voltage increases to its reference within 30ms. There is no overshoot in the actual V_2 because the parameters of the PI controller are designed only to ensure the stability, but not to

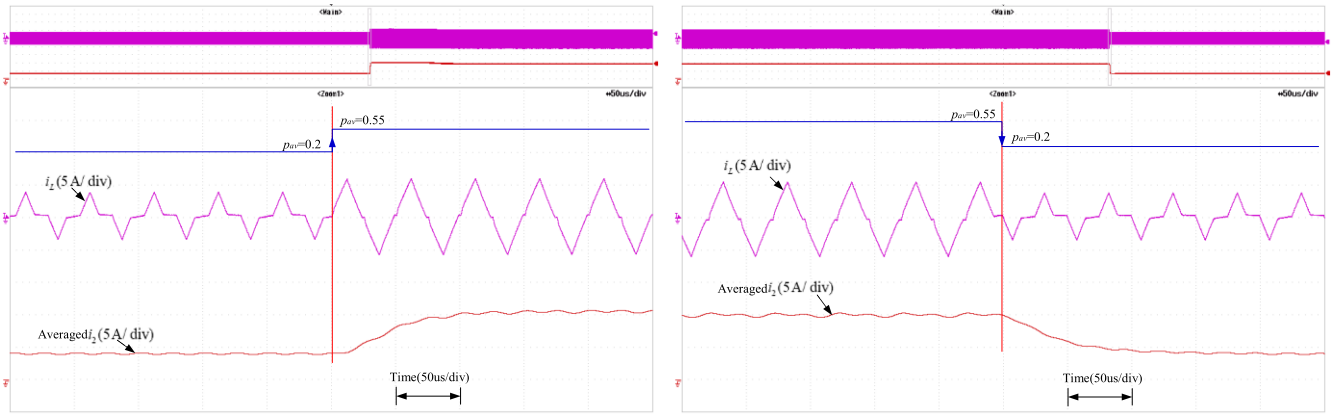

FIGURE 7. Experimental results of DAB converter with step change of average power reference. (a) From 0.2 to 0.55, (b) From 0.55 to 0.2.

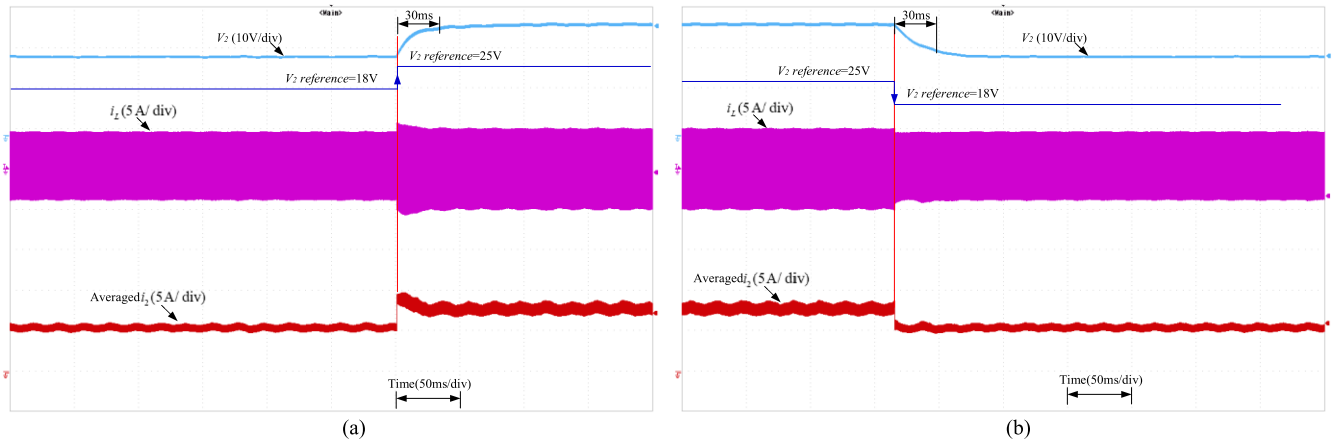

FIGURE 8. Experimental results of DAB converter with step change of output voltage reference. (a) From 18V to 25V, (b) From 25V to 18V.

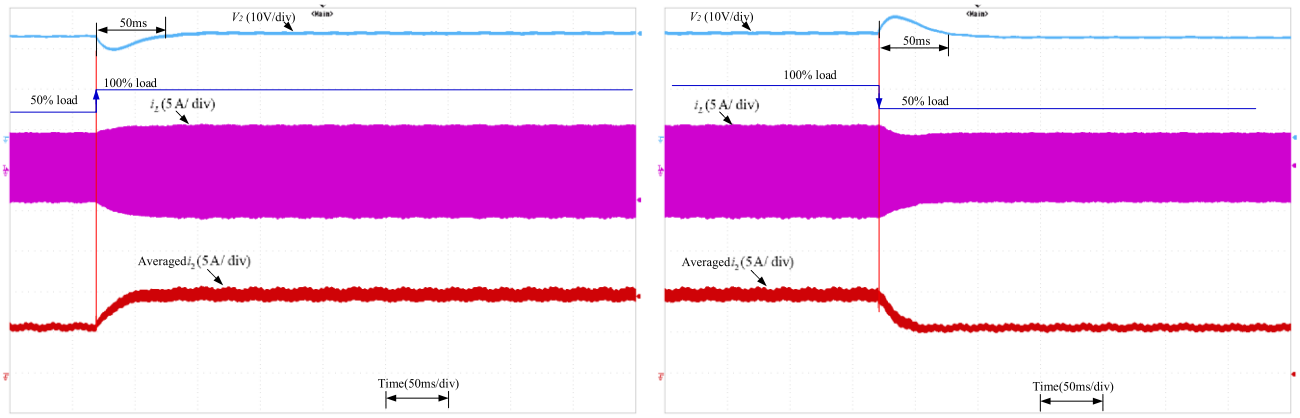

FIGURE 9. Experimental results of DAB converter with step change of load resistance. (a) From 50% to 100%, (b) From 100% to 50%.

pursue an extreme dynamic performance. More importantly, there is no transient overshoot or delay in the inductor current. The correctness of the built model of the DAB converter is verified once again and it means even though the actual inductor current is not controlled in a closed-loop way, it is still controllable and the safety and reliability of the DAB converter are ensured.

The second way to evaluate the dynamic performance of the voltage closed-loop control approach is to jump the resistance of the load from 100% to 50% and from 50% to 100%, respectively. The corresponding experimental waveforms are shown in Fig. 9(a) and (b), respectively. From Fig. 9, the actual inductor current varies immediately and the actual averaged i_2 varies very fast as well. After about 50ms, the actual secondary DC side voltage reaches to the new reference and there is no overshoot in the both cases. It achieves a good dynamic performance. During the dynamic process, the actual inductor current is always under control, there is no overshoot or additional transient process in it.

Moreover, the experimental waveforms of the DAB dc-dc converter driven by the CPTS control under reverse mode are tested and shown in Fig. 10. Fig. 10 (a), (b) show the open-loop experimental waveforms with different power reference. When the transfer power vary in a wide range, v_{h2} is always ahead of v_{h1} and both i_1 and i_2 are less than zero or equal to zero, it means the actual power flows from V_2 to V_1 and the dual side flow back currents are completely eliminated. The waveforms of all of the variables under reverse mode are similar with the ones under forward mode shown in [13]. Fig. 10 (c) and (d) show the closed-loop experimental waveforms under reverse mode. The dynamic performance under reverse mode is quite similar with that under forward mode.

From the both dynamic experimental results, the following two aspects are verified. (1) The unique feature of CTPS, that is, the relationship between the inductor current and the three phase shifts is zero-order, is correct. (2) It is not necessary to control the inductor current in a closed-loop way and the inductor current is always under control even it is not directly controlled. (3) The direct power based control approach achieves a good control performance and it significantly simplify the closed-loop control configuration.

TABLE 2. Dynamic response data of several control strategies.

		TVL	LCFF	MPC	VDPC	Proposed
Voltage ref. step	Response time (ms)	162	116	84	44	30
	Overshoot (p.u.)	0	0	0	0	0
Load step	Response time (ms)	250	159	150	100	50
	Overshoot (p.u.)	0.08	0.16	0.12	0.05	0.1

Furthermore, the efficiency of the DAB converter with the CTPS is test with V_1=100V and V_2=25V. The corresponding efficiency curve is shown in Fig.11. The efficiency increases gradually with the increase of the transfer power first and when the power is greater than 0.7, the efficiency decreases gradually with the increase of the transfer power. The maximum efficiency is about 96%.

Finally, the dynamic performance of the proposed approach is compared with several of several closed-loop control strategies of the DAB converter with SPS. In [22], the performance of the traditional voltage closed-loop control (TVL), the load current feed-forward control (LCFF), the model-based phase-shifted control (MPC) and the virtual direct power control (VDPC) are tested and compared with each other. We read the dynamic response data of the output voltage step change and load step change of these strategies from [22] and listed them together with those of the proposed one in Table 2. From Table 2, the dynamic response time and overshoot voltage of the proposed strategies is better than those of CVL, LCFF, MPC and is similar with that of VDPC. It means the proposed approach realizes the closed-loop control of the output voltage with a good steady-state and dynamic performance.

In addition, the reason that the dynamic performance of the CVL, LCFF, MPC is not so good is analysed below. From the built linear model of the DAB converter based on SPS modulation using the fundamental analysis method, the transfer function of phase shift to inductor current is at

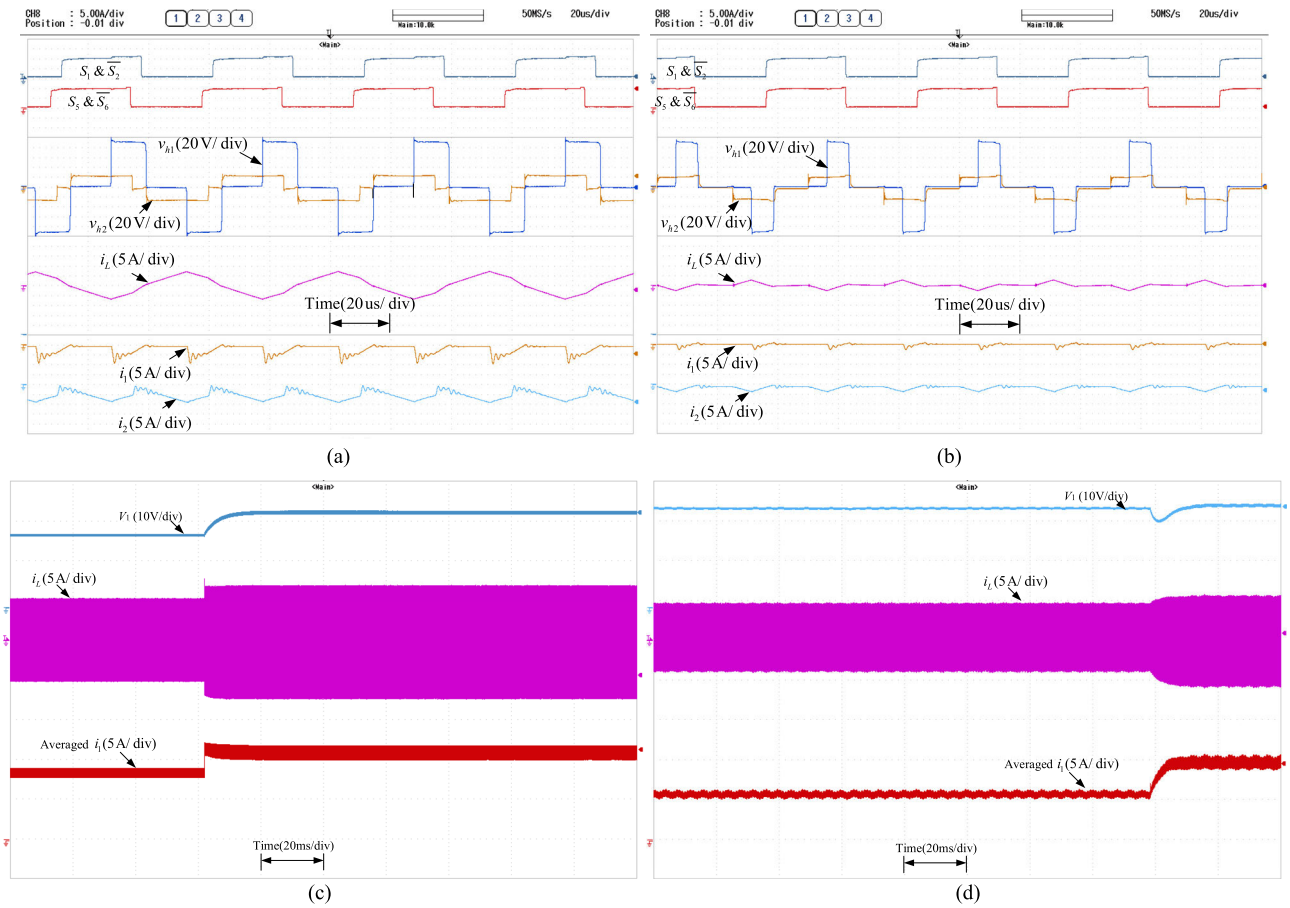

FIGURE 10. Experimental results of CTPS control under reverse mode. (a) p_{av} greater than pcri, (b) p_{av} less than pcri, (c) voltage reference step, (d) load step.

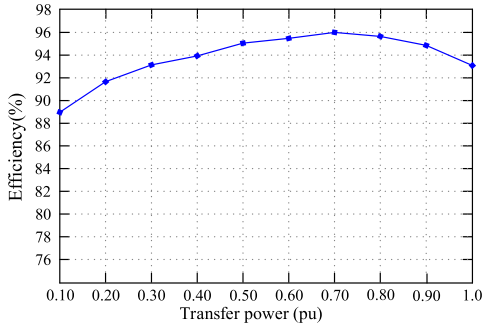

FIGURE 11. Distribution curves of efficiency as a function of transfer power.

least three-order. However, all of these control strategies are based on the average model and do not consider the transient relationship between the phase shift and the inductor current. It slows the dynamic performance.

VI. CONCLUSION

The established average state-space model of DAB DC-DC converter with the CTPS proves that the DAB converter becomes a zero-order system and it makes the closed-loop control of the DAB converter easier. The direct power control based on the expression of the average transfer power as a function of the three phase shifts achieves the good dynamic performance in the two application scenarios of connecting the DAB converter to the DC microgrid or severing as a DC source supply. The research work is helpful to increase the practicability of the CTPS and ensures that the CTPS is able to apply in the actual systems to best develop its advantages of the good current characteristics and full soft-switching operation.

REFERENCES

[1] P. Jain, M. Pahlevaninezhad, S. Pan, and J. Drobnik, "A review of high-frequency power distribution systems: For space, telecommunication, and computer applications," *IEEE Trans. Power Electron.*, vol. 29, no. 8, pp. 3852–3863, Aug. 2014.

[2] L. Xue, Z. Shen, D. Boroyevich, P. Mattavelli, and D. Diaz, "Dual active bridge-based battery charger for plug-in hybrid electric vehicle with charging current containing low frequency ripple," *IEEE Trans. Power Electron.*, vol. 30, no. 12, pp. 7299–7307, Dec. 2015.

[3] F. J. Wu, S. Fan, X. Li, and S. Luo, "Bidirectional buck–boost current-fed isolated DC–DC converter and its modulation," *IEEE Trans. Power Electron.*, vol. 35, no. 5, pp. 5506–5516, May 2020.

[4] J. Liu, J. Yang, J. Zhang, Z. Nan, and Q. Zheng, "Voltage balance control based on dual active bridge DC/DC converters in a power electronic traction transformer," *IEEE Trans. Power Electron.*, vol. 33, no. 2, pp. 1696–1714, Feb. 2018.

[5] F. Wu, S. Fan, and S. Luo, "Small-signal modeling and closed-loop control of bidirectional buck-boost current-fed isolated DC–DC converter," *IEEE Trans. Ind. Electron.*, vol. 68, no. 5, pp. 4036–4045, May 2021.

[6] S. H. Luo and F. J. Wu, "Hybrid modulation strategy for IGBT-based isolated dual-active-bridge DC–DC converter," *IEEE J. Emerg. Sel. Topics Power Electron.*, vol. 6, no. 3, pp. 1336–1344, Sep. 2018.
[7] B. Zhao, Q. Song, W. Liu, and W. Sun, "Current-stress-optimized switching strategy of isolated bidirectional DC–DC converter with dual-phase-shift control," *IEEE Trans. Ind. Electron.*, vol. 60, no. 10, pp. 4458–4467, Oct. 2013.
[8] N. Hou, W. Song, and M. Wu, "Minimum-current-stress scheme of dual active bridge DC–DC converter with unified phase-shift controll," *IEEE Trans. Power Electron.*, vol. 31, no. 12, pp. 8552–8561, Dec. 2016.
[9] J. Huang, Y. Wang, Z. Li, and W. Lei, "Unified triple-phase-shift control to minimize current stress and achieve full soft-switching of isolated bidirectional DC–DC converter," *IEEE Trans. Ind. Electron.*, vol. 63, no. 7, pp. 4169–4179, Jul. 2016.
[10] A. Tong, L. Hang, G. Li, X. Jiang, and S. Gao, "Modeling and analysis of a dual-active-bridge-isolated bidirectional DC/DC converter to minimize RMS current with whole operating range," *IEEE Trans. Power Electron.*, vol. 33, no. 6, pp. 5302–5316, Jun. 2018.
[11] V. Karthikeyan and R. Gupta, "Zero circulating current modulation for isolated bidirectional dual-active-bridge DC–DC converter," *IET Power Electron.*, vol. 9, no. 7, pp. 1553–1561, Jul. 2016.
[12] Y. Chu and S. Wang, "Bi-directional isolated DC-DC converters with reactive power loss reduction for electric vehicle and grid support applications," in *Proc. IEEE Transp. Electrific. Conf. Expo (ITEC)*, Dearborn, MI, USA, Jun. 2012, pp. 1–6.
[13] F. J. Wu, F. Feng, and H. B. Goay, "Cooperative triple-phase-shift control for isolated DAB DC–DC converter to improve current characteristics," *IEEE Trans. Ind. Electron.*, vol. 66, no. 9, pp. 7022–7031, Sep. 2019.
[14] H. Bai, Z. Nie, and C. Mi, "Experimental comparison of traditional phase-shift, dual-phase-shift, and model-based control of isolated bidirectional DC–DC converters," *IEEE Trans. Power Electron.*, vol. 25, no. 6, pp. 1444–1449, Jun. 2010.
[15] C. Zhao, S. D. Round, and J. W. Kolar, "Full-order averaging modelling of zero-voltage-switching phase-shift bidirectional DC–DC converters," *IET Power Electron.*, vol. 3, no. 3, pp. 400–410, 2010.
[16] H. Qin and J. W. Kimball, "Generalized average modeling of dual active bridge DC–DC converter," *IEEE Trans. Power Electron.*, vol. 27, no. 4, pp. 2078–2084, Apr. 2012.
[17] I. R. Erni, E. Vidal-Idiarte, J. Calvente, and L. Guasch-Pesquer, "Small signal modelling for variable frequency control with maximum efficiency point tracking of DAB converter," *IEEE Access*, vol. 9, pp. 85289–85299, 2021.
[18] J. A. Mueller and J. W. Kimball, "Modeling dual active bridge converters in DC distribution systems," *IEEE Trans. Power Electron.*, vol. 34, no. 6, pp. 5867–5879, Jun. 2019.
[19] H. Bai, C. Mi, C. Wang, and S. Gargies, "The dynamic model and hybrid phase-shift control of a dual-active-bridge converter," in *Proc. 34th Annu. Conf. IEEE Ind. Electron.*, Nov. 2008, pp. 2840–2845.
[20] F. An, W. Song, K. Yang, N. Hou, and J. Ma, "Improved dynamic performance of dual active bridge DC–DC converters using MPC scheme," *IET Power Electron.*, vol. 11, no. 11, pp. 1756–1765, Sep. 2018.
[21] S. Dutta, S. Hazra, and S. Bhattacharya, "A digital predictive current-mode controller for a single-phase high-frequency transformer-isolated dual-active bridge DC-to-DC converter," *IEEE Trans. Ind. Electron.*, vol. 63, no. 9, pp. 5943–5952, Sep. 2016.
[22] W. Song, N. Hou, and M. Wu, "Virtual direct power control scheme of dual active bridge DC–DC converters for fast dynamic response," *IEEE Trans. Power Electron.*, vol. 33, no. 2, pp. 1750–1759, Feb. 2018.
[23] S. P. Engel, N. Soltau, H. Stagge, and R. W. Doncker, "Dynamic and balanced control of three-phase high-power dual-active bridge DC–DC converters in DC-grid applications," *IEEE Trans. Power Electron.*, vol. 28, no. 4, pp. 1880–1889, Apr. 2013.
[24] S. K. Gurumurthy, S. K. Gurumurthy, S. K. Bhanderi, Z. Yang, and P. Joebges, "Port controlled Hamiltonian modeling and IDA-PBC control of dual active bridge converters for DC microgrids," *IEEE Trans. Ind. Electron.*, vol. 66, no. 11, pp. 9065–9075, Nov. 2019.
[25] S. P. Engel, N. Soltau, H. Stagge, and R. W. Doncker, "Improved instantaneous current control for high-power three-phase dual-active bridge DC–DC converters," *IEEE Trans. Power Electron.*, vol. 29, no. 8, pp. 4067–4077, Aug. 2014.

YONG DAI received the Ph.D. degree in mechanical and electronic engineering from the Harbin Institute of Technology (HIT), Harbin, China, in 2003.

Since 2003, he has been with the Department of Mechanical and Electronic Engineering, HIT, where he is currently a Lecturer. His research interest includes the area of industrial robot and application.

SUHUA LUO received the M.S. and Ph.D. degrees in optics from the Harbin Institute of Technology (HIT), Harbin, China, in 2004 and 2009, respectively.

Since 2009, she has been with the Department of Physics, HIT, where she is currently a Lecturer. Her research interests include the area of information detection, processing, optical holographic storage, and photovoltaic generation systems.

ZHONGWEI LI (Member, IEEE) received the Ph.D. degree in electrical engineering from the Harbin Institute of Technology (HIT), Harbin, China, in 2006.

Since 2006, he has been with the Department of Electrical Engineering, HIT, where he is currently an Associate Professor. His research interests include the area of industrial internet and energy internet.